Materials Science and Engineering C 50 (2015) 24–30

Contents lists available at ScienceDirect

Materials Science and Engineering C

journal homepage: www.elsevier.com/locate/msec

Evaluating the effects of hydroxyapatite coating on the corrosion behavior of severely deformed 316Ti SS for surgical implants

Mansour Mhaede [a,b,*], Aymen Ahmed [a], Manfred Wollmann [a], Lothar Wagner [a]

[a] Institute of Materials Science and Engineering, Clausthal University of Engineering, Agicolastr.6, 38678 Clausthal-Zellerfeld, Germany
[b] Faculty of Engineering, Zagazig University, 44519 Zagazig, Egypt

ARTICLE INFO

Article history:
Received 13 October 2014
Received in revised form 8 January 2015
Accepted 30 January 2015
Available online 31 January 2015

Keywords:
316Ti SS
Cold rolling
HA coating
Corrosion

ABSTRACT

The present work investigates the effects of severe plastic deformation by cold rolling on the microstructure, the mechanical properties and the corrosion behavior of austenitic stainless steel (SS) 316Ti. Hydroxyapatite coating (HA) was applied on the deformed material to improve their corrosion resistance. The martensitic transformation due to cold rolling was recorded by X-ray diffraction spectra. The effects of cold rolling on the corrosion behavior were studied using potentiodynamic polarization. The electrochemical tests were carried out in Ringer's solution at 37 ± 1 °C. Cold rolling markedly enhanced the mechanical properties while the electrochemical tests referred to a lower corrosion resistance of the deformed material. The best combination of both high strength and good corrosion resistance was achieved after applying hydroxyapatite coating.

1. Introduction

Metallic materials are widely used in medical applications as implants to restore lost functions or replace organ functioning below acceptable levels [1]. Implantation applications have been markedly increased; every year over 270,000 hip replacements are performed in the United States [2]. Moreover, by 2030, the demand for primary total hip arthroplasties is estimated to grow by 174% to 572,000. The demand for hip revision procedures is projected to marked growth in the next decades [2,3]. Surgical implants such as hip and knee joint implants usually fail within a period of about 10–15 years of use, which leads to revision surgery in order to recover the functionality of the system [4]. The reasons for their failure include degradation, design and surgical issues [5]. The commonly applied metallic biomaterials for orthopedic applications in clinical practice are stainless steels, cobalt–chromium and titanium-based alloys [6,7]. These materials are more suitable for load-bearing applications compared with ceramics or polymeric materials, mainly due to their combined high mechanical strength and fracture toughness [8]. However, corrosion of metallic implants is one of the most critical issues in their use because it could negatively affect their biocompatibility and mechanical integrity. The success of implants in the human body depends on many factors such as biocompatibility and biofunctionality in the environment wherein the implants are placed.

The necessity of cost reduction in public health services makes stainless steel as the most economical option of metals used in orthopedic surgery [9,10]. It is widely applied for temporary implantation, although it is also used as permanent implants in developing countries [11]. Stainless steel is used both in artificial knee and hip joints, bone plate or screw [12,13], such implants require high strength. The strength of stainless steel could be improved through grain refinement [14]. The ultrafine grained stainless steel exhibited excellent strength and elongation [15,16]. Such modification of the mechanical properties is mainly due to the partial transformation of austenite to martensite ($\gamma \rightarrow \alpha'$) and by the extra dislocations introduced by strain [17,18]. The plastically deformed-high strength austenitic stainless steel AISI 304 has a lower corrosion resistance compared to the coarse grained materials [18]. Both the thickness and composition of passive films are likely to be modified in many ways by plastic deformation [19]. Moreover, the aggressive corrosive biological environment leads to localized corrosion attack in long-term applications of stainless steel implants, causing premature failure [20]. Studies on retrieved implants showed that more than 90% of the failure of 316L SS-implants is due to localized electrochemical cells resulting in pitting attack, or crevice corrosion at the interface between a plate and a locking screw [21]. The resulting corrosion products may cause a local inflammatory response, finally leading to the cessation of bone formation, synovitis, and loosening of artificial joint implants [22]. Therefore, the corrosion resistance of the implants must be enhanced. Hydroxyapatite (HA) coatings are commonly used to coat acetabular components, knee prosthesis, pin/screw components and dental implants [23–25]. Hydroxyapatite (HA) coatings are also widely employed to enhance the osseointegration of orthopedic and dental implants [26]. These coatings [$Ca_5(PO_4)_3OH$] consist of 39.9%

* Corresponding author at: Institute of Materials Science and Engineering, Clausthal University of Engineering, Agicolastr.6, 38678 Clausthal-Zellerfeld, Germany.
E-mail addresses: mansour.mhaede@yahoo.com, mansour.mhaede@tu-clausthal.de (M. Mhaede).

http://dx.doi.org/10.1016/j.msec.2015.01.093
0928-4931/

Table 1
Chemical composition of SS 316Ti in wt.%.

Element	C	Si	Mn	P	S	Cr	Mo	Ni	N	Ti
wt.%	0.024	0.50	1.57	0.038	0.015	17.75	1.949	10.2	0.080	0.23

Ca, 18.5% P, 41.4% O and 3.4% OH (values in weight percentage) and the Ca/P molar ratio is 1.67. This chemical composition resembles the mineral component of human bones and hard tissues [27].

The present study aims at investigating the effects of plastic deformation by cold rolling on the mechanical properties and corrosion behavior of 316Ti SS. The Ti-content of this SS reacts with carbon to form titanium carbides which limits the formation of chromium-rich carbides and prevents precipitation of grain boundary carbides that may cause corrosion reactions [28]. Corrosion tests were carried out in Ringer's solution as a simulated body fluid. In addition, hydroxyapatite coating (HA) was applied to the deformed and the as-received materials to enhance their corrosion resistance.

2. Experimental procedures

Austenitic stainless steel 316Ti (X6CrNiMoTi17-12-2) was received in plate form with thickness of 30 mm, chemical composition is given in Table 1. The material was cold-rolled to different deformation degrees. The deformation degree is defined as $\varphi = \ln(A_0 / A)$, where A_0 is the starting cross sectional area and A is the final cross sectional area. Hardness measurements, via Vickers hardness tester (98.07 N for 15 S), were done on material cold rolled to definite deformation degrees. The microstructure development was recorded using an optical microscope (Model: Zeiss Axioskop). The martensitic transformation after cold rolling was recorded by X-ray diffraction spectra (XRD) operated with Co-Kα, D5000 diffractometer. Samples of 20 × 10 × 2 mm were cut from the as-received and the deformed materials. The samples were ground to 600 grit using silicon carbide (SiC) papers followed by ultrasonic cleaning in ethanol bath. The samples were then coated with hydroxyapatite coating (HA). HA coating was prepared using chemical deposition method. This method has an advantage of depositing a homogenous HA coating on dental and orthopedic implants with complex geometry (internal cavity) or macro-porosities. Moreover, this coating method is simple and inexpensive for use in the biomaterials industry. The samples were firstly soaked in 2 M KOH solution for 2 h at 90 °C in order to prevent the cracking caused by the evolution of H_2 during the dissolution of the substrate [29]. The HA coating solution was prepared from 0.69 M KOH, 0.49 M EDTA (Ethylene diamine tetra acetic acid), 0.15 M KH_2PO_4 and 1.14 M $CaNO_3 \cdot H_2O$. The chemical bath deposition was performed in 50 ml beaker, in which the SS samples were vertically suspended. The beaker was heated in a water bath up to 70 °C for 2 h, after that the temperature was slowly raised to 95 °C. After 3 h of deposition, the substrates were removed, washed in water, and air-dried at room temperature. The process was repeated with the same substrates to get thicker HA coatings. The surface morphology of the formed coating and the Ca/P ratio were identified by scanning electron microscopy (SEM) "HITACHI X-50" and energy dispersive X-ray spectroscopy (EDX) using UltraDry Compact EDS Detector from Thermo Scientific.

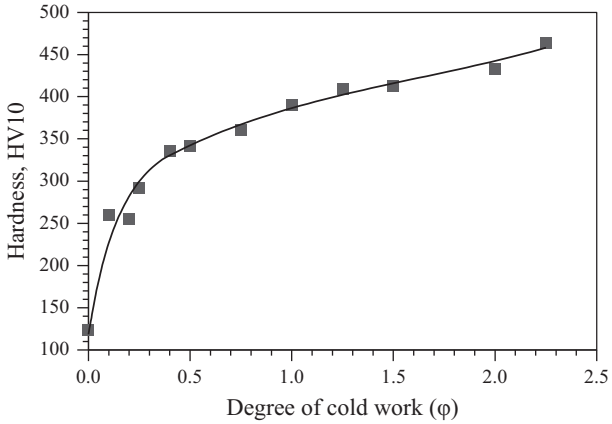

Fig. 2. Relation between hardness and deformation degree in cold rolling.

The electrochemical polarization measurements were carried out in a round bottom polarization cell using VersaSTAT3 potentiostat from the Princeton Applied Research company, interfaced to a computer. The tests were conducted according to ASTM G5-94 [30]. Ringer's solution was used as an electrolyte to simulate the human body fluid. It was prepared using laboratory grade chemicals and distilled water. The composition of the used Ringer's solution was (in gm/l) 8.6 NaCl, 0.3 KCl, and 0.48 $CaCl_2$. Freshly prepared solution was used for each experiment. A conventional three-electrode cell was used. The counter electrode was a platinum sheet and all the potential data were reported relative to a saturated calomel reference electrode (SCE). The luggin capillary was placed close to a working electrode, which had an area of 1 cm^2. The electrolyte temperature of 37 ± 1 °C was maintained using a heating mantle. All the potentiodynamic polarization experiments were conducted after stabilization of the free corrosion potential. A scan rate of 1 mV/s was applied due to noisy current behavior of steel at low over-potentials [31]. The corrosion rate was determined using the Tafel extrapolation method. The surfaces of the corroded samples were examined using SEM and light microscope.

The Corrosion rate (in mpy), which was extracted from the extrapolation of the Tafel lines of each polarization curve, is calculated by the following equation:

$$CR = \frac{I_{corr} \times K \times EW}{\rho \times A}$$

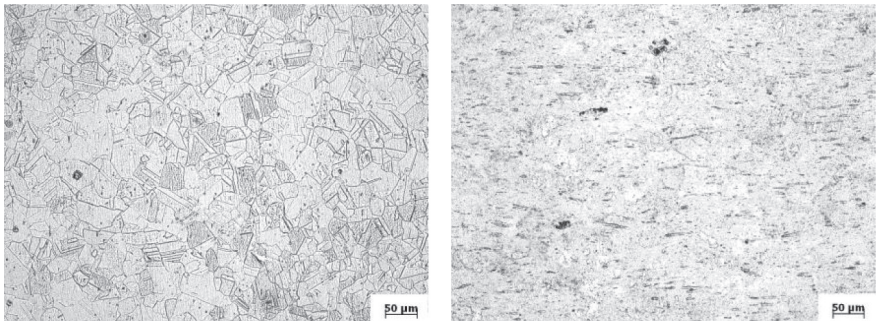

a) φ= 0 b) φ= 2.25

Fig. 1. Microstructure of SS 316Ti.

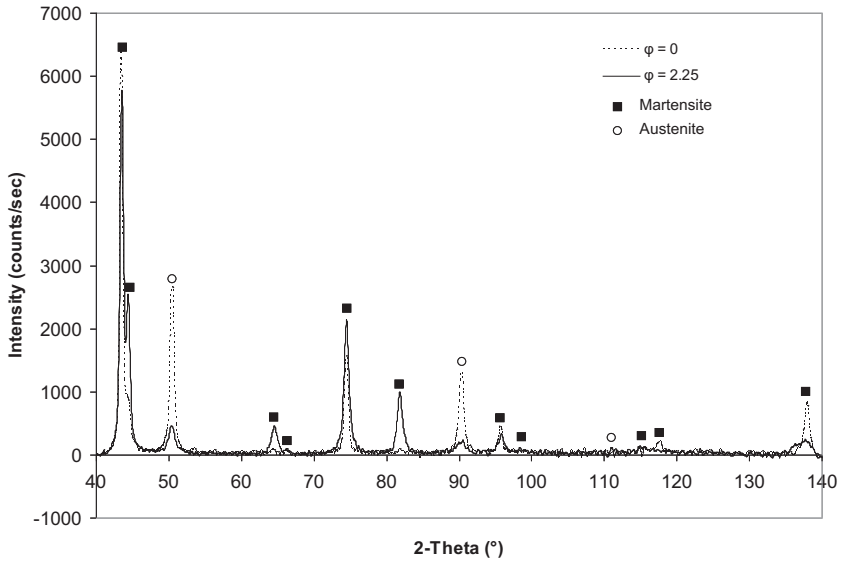

Fig. 3. X-ray diffraction spectra of non-deformed ($\varphi = 0$) and highly deformed ($\varphi = 2.25$) SS 316Ti.

where I_{corr} = corrosion current density in Ampere (A), K = constant that defines the units of corrosion rate (1.288×105 mils/A cm year), EW = equivalent weight in (g/equivalent), ρ = density (7.99 g/cm^3) and A = sample area in cm^2. The equation indicates that, corrosion rate is directly proportional to corrosion current density.

3. Results and discussion

3.1. Material characterization

The microstructures of 316Ti SS before and after cold rolling are illustrated in Fig. 1. Fig. 1a represents a typical equiaxed grained

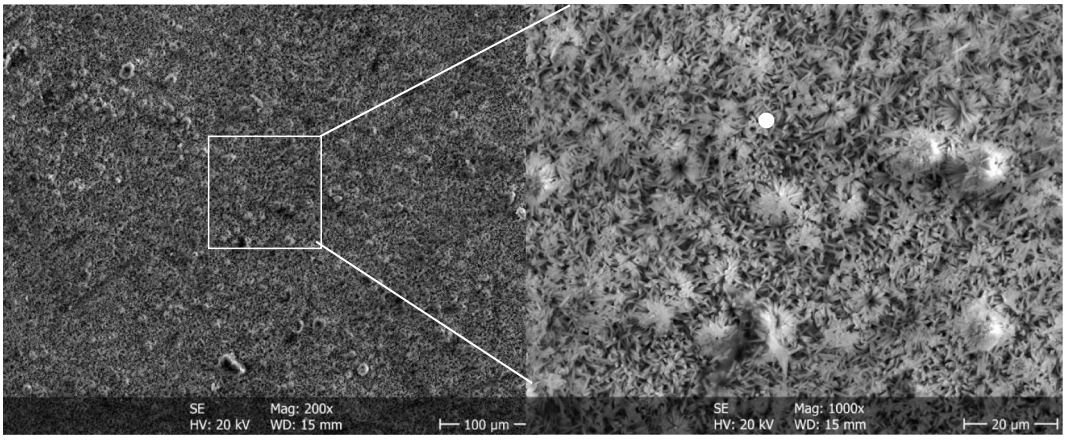

(a)

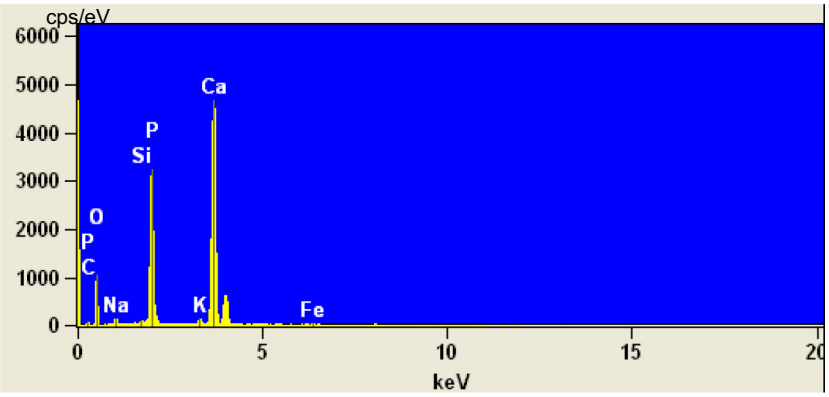

(b)

Fig. 4. (a) Appearance of HA coating, and (b) corresponding EDX analysis of HA coating (bright marked circle).

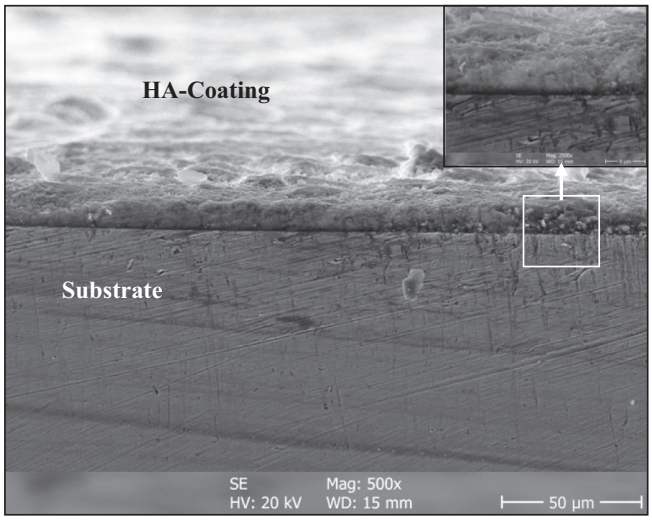

Fig. 5. SEM micrograph of HA coating (cross-section).

austenitic microstructure of the non-deformed ($\varphi = 0$) condition, after cold rolling ($\varphi = 2.25$) the grains were highly deformed and elongated in rolling direction (Fig. 1b). The average grain size of the as-received material is about 38 µm. It was hard to calculate the grain size of the deformed material. The effect of cold rolling on the hardness is shown in Fig. 2. With an increase in the degree of deformation by cold rolling, the hardness increased significantly from about 125 to 460 HV10. The ductility of the non-deformed material ($\varphi = 0$) was 0.44 (strain to fracture, $\varepsilon_F = \ln(A_o / A_F)$). After deformation, the material still had a ductility of 0.19 that ensures a suitable workability. Moreover, the deformed material exhibited higher strength values, which are suitable for higher fatigue lifetime. This strong strain hardening is mainly due to the very low stacking fault energy (SFE) in austenitic stainless steels in which plastic deformation is characterized by the dissociation of perfect dislocations in Shockley partial dislocations and the formation of wide stacking faults [32,33]. Furthermore, part of the observed strengthening may be caused by strain-induced transformation of the austenite to martensite as shown in Fig. 3 [34].

3.2. Coating characterization

Fig. 4a shows a SEM micrograph of the formed HA coating on a sample deformed at $\varphi = 2.25$. The HA coating exhibited a needle-like morphology. The obtained coating was homogeneous, dense and crack-free, however the SEM micrographs revealed the presence of micropores. The underlying substrate material was completely covered by the coating. The cross-section of the coating in Fig. 5 showed a uniform layer with a relatively close contact at the interface between substrate and coating. Moreover, the interface between HA coating and SS substrate, as presented in Fig. 5, is similar to the SEM micrographs of the Ti substrate samples after coating by HA using a chemical bath method [35]. The coating/substrate interface can be improved by post heat treatments that improve bonding through enhanced diffusion at the interface [36,37]. The achieved HA coating had a layer thickness of about 15 µm. The HA-coated samples showed a rough topography. The surface roughness parameters (R_{max} and R_a) of the grinded and HA-coated surfaces are presented in Table 2. The HA-coated surface revealed markedly

Table 2
Roughness values.

Surface conditions	R_{max}, µm	R_a, µm
Grinded	0.55	0.05
HA	4.93	0.63

Table 3
Elemental composition of the HA coating after chemical deposition (EDX analysis).

Element	C–K	O–K	Na–K	P–K	K–K	Ca–K	Si–K	Fe–K
atom.%	3.80	58.60	2.20	13.10	0.30	21.40	0.10	0.20

higher roughness values compared to the grinded surface. Surface roughness is considered as a very important factor for implant/tissue interaction and its influence on the biocompatibility in clinical use [38,39]. The EDX analysis (Fig. 4b and Table 3) reveals that HA coating had an average Ca/P ratio of 1.63, which is close to the Ca/P ratio (1.67) of stoichiometric HA [$Ca_{10}(PO_4)_6(OH)_2$] [40]. After deposition of the HA, crystal structure of the coating was investigated by XRD-ray operated with Co-Kα radiation. XRD spectra (Fig. 6) of the formed coating confirmed the formation of HA coexisting with CaP phase. The crystalline HA-phase was observed at the highest peak of $2\theta = 30°$, which confirms that HA was the dominant phase in the coating.

3.3. Corrosion behavior

Fig. 7 shows the potentiodynamic polarization curves of non-deformed ($\varphi = 0$) and deformed specimens. It is obvious that increasing the deformation degree led to a clear shift in the corrosion potential (E_{corr}) to the negative direction, and an increase in the anodic current density (I_{corr}). Table 4 represents the electrochemical characteristics of the different tested conditions. The corrosion current density I_{corr} of the non-deformed material ($\varphi = 0$) increased from 1128 to 9980 nA·cm^{-2} after deformation at $\varphi = 2.25$. Correspondingly, the corrosion rate of the non-deformed material ($\varphi = 0$) increased from 0.302 to 3.09 mpy after deformation at $\varphi = 2.25$. The increased electrochemical activity by increasing the deformation degree might be related to the increased martensite content due to deformation. The martensite phase could act as an anode in an electrochemical cell and is thereby prone to selective dissolution. Chloride ions are adsorbed preferentially on martensite locations and then react with the surface film. This leads to destruction of the surface film and delays its restoration. Metallographic observations (Fig. 8) of sample surfaces after electrochemical tests showed numerous corrosion pits. Generally, corrosion resistance of stainless steels is achieved by dissolving a sufficient amount of chromium in iron to produce a coherent, adherent, insulating and regenerating chromium oxide protective film (Cr_2O_3) on the surface. This passive film of chromium oxide formed in air at room temperature is only about 1–2 nm. Pitting corrosion is the result of the local destruction of the passive film and subsequent corrosion of the steel underneath this layer. The micrographs in Fig. 7 indicated that the pit initiation frequency increased with the deformation degree. The pit formation is influenced by many factors such as martensite content, dislocation density and internal stresses [41,42]. A. Barbucci et al. [43] have

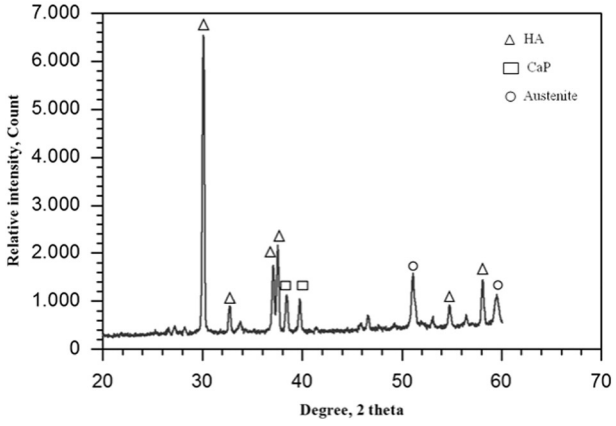

Fig. 6. X-ray diffraction spectra of HA coating formed on the surface of SS 316Ti.

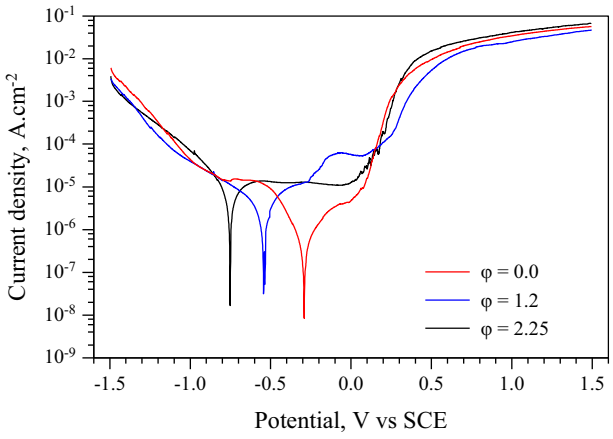

Fig. 7. Potentiodynamic polarization curves of the non-deformed ($\varphi = 0$) and deformed ($\varphi = 1.2$ and $\varphi = 2.25$) SS 316Ti in Ringer's solution at 37 °C.

Table 4
Results of the electrochemical tests of SS 316Ti cold rolled at different deformation degrees.

Deformation degree	Corrosion current density, I_{corr} ($nA \cdot cm^{-2}$)	Corrosion potential E_{corr} (mV)	Corrosion rate mpy
$\varphi = 0.0$	1128	−291	0.302
$\varphi = 1.2$	6730	−541	1.58
$\varphi = 2.25$	9980	−752	3.09
$\varphi = 0.0 + HA$	370	−184	0.275
$\varphi = 2.25 + HA$	325	−677	0.167

related the pit initiation to the passive film stability, which is influenced by cold deformation. The increased number of pits by increased cold work suggests a much higher defective oxide film in deformed material. The surface defects may lead to a selective Fe dissolution and diminish the protection of the substrate by the film, i.e., they increase its apparent conductivity. Previous studies reported that the equilibrium ferrite/austenite structures could promote galvanic corrosion with dissolution of ferrite in open-circuit conditions [44,45]. Moreover, it is reported that the inclusions are likely to affect the pitting initiation [46].

The effect of HA coating on the corrosion behavior, in terms of potentiodynamic polarization, is illustrated in Fig. 9. The figure shows the potentiodynamic polarization curves of the non-deformed ($\varphi = 0$) + HA coating and deformed ($\varphi = 2.25$) + HA coating. It is clear that HA coating resulted in a significant reduction of the corrosion current density. The corrosion potential E_{corr} shows a relative shift to the positive direction. More interestingly, the cathodic and anodic currents of the deformed material ($\varphi = 2.25$) + HA coating were lower than those of the non-deformed material ($\varphi = 0$) + HA coating. Correspondingly, the values of I_{corr} and corrosion rate calculated based on Tafel extrapolation, of the deformed ($\varphi = 2.25$) + HA coating, were relatively lower than those of the non-deformed ($\varphi = 0$) + HA coating (Table 4). Introducing HA coating on the surface of the deformed material ($\varphi = 2.25$) led to a reduction of the corrosion current density and corrosion rate from 9980 $nA \cdot cm^{-2}$ and 3.09 mpy to 328 $nA \cdot cm^{-2}$ and 0.167 mpy, respectively. The progressive enhancement of the corrosion resistance after HA coating is related to the fact that HA is a non-interactive ceramic material. Accordingly, HA coating forms a barrier that prevents ion release from the substrate hence provides a good protection against corrosive environment.

The coating thickness is an effective important factor influencing adhesion and corrosion resistance. B. Aksakal et al. [47] found that adhesion and corrosion resistance decreased with increasing coating thickness on 316L SS. The authors observed increased surface cracks after thicker HA coatings. The number of cracks reached a significant level when the thickness was more than 40 μm and the highest corrosion susceptibility was found on 72 μm HA-coated 316L SS. Such cracks may lead to loosening of the implants. Moreover, the bonding strength of thicker HA coatings was lower than that of thinner ones. Bonding strength of HA coatings decreased with increasing coating thickness. After the corrosion tests, it was observed that the bonding strength was reduced. S. Sonmenz et al. [48] stated that the micro-scale HA-coated Mg substrates were more corrosion resistant than the nano-scale HA-coated substrates. Thicker coatings often exhibited porosity that weakened the interfacial strength and provided an easy path for adhesion failure. The coating with higher crystallinity and fewer defects may be preferentially considered. The nucleation, growth of crystals onto the substrate, dissolution and precipitation rates of HA coatings are critically dependent on the crystal structure developed in the coatings. HA coatings with higher crystallinity yielded a decreased dissolution rate [49] and higher rates of cell proliferation [50]. Darimont et al. [51] concluded that implants in trabecular and cancellous bone require coatings with a very high crystallinity. Another study by W. Xue et al. [52] deduced that the HA coating with high crystallinity showed the lower dissolution compared to the low crystallinity coating. They found that, after 3 months from implantation, the high crystallinity coating showed the higher shear strength and remained integrated. Whereas the separation of the coating fragments was clearly observed in the low crystallinity coating. In brief, the high crystalline HA coating is suitable for long-term implantation and the low crystalline coating has superiority in promoting faster initial bone fixation [53].

The formation of the passive film was found to occur with wider potential range for both HA-coated materials in comparison with the uncoated materials. This indicates that the passivation through the HA coating leads to a significant enhancement of the passivation properties of the surface oxide film [54]. The passive film prevents the dissolution of the substrate into the electrolyte. SEM micrographs of the HA-coated samples after corrosion tests revealed the presence of localized corrosion pits (Fig. 10). There was no significant difference in the size of the formed corrosion pits on the HA-coated surfaces of non-deformed and

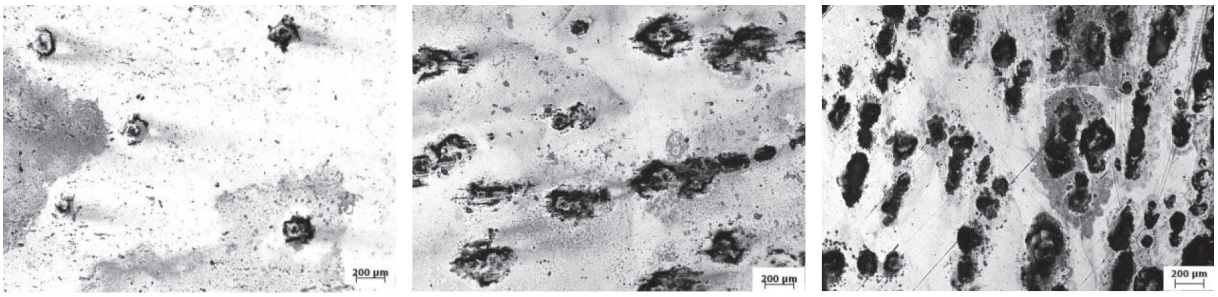

Fig. 8. Optical micrographs revealing corrosion pit formation after potentiodynamic polarization of uncoated SS 316Ti (a) $\varphi = 0$, (b) $\varphi = 1.2$ and (c) $\varphi = 2.25$.

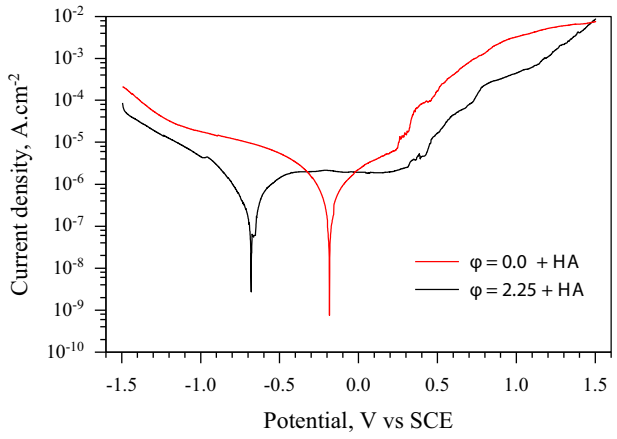

Fig. 9. Potentiodynamic polarization curves of the HA-coated SS 316Ti in Ringer's solution at 37 °C.

deformed samples. However, pitting corrosion had been gratefully controlled in HA-coated material, i.e., the number of the formed pits on the HA-coated surfaces after corrosion tests was clearly lower than those observed on the uncoated samples. Appearance of these pits confirms the fact that even the HA-coated samples suffer corrosion but with a lower corrosion rate. The presence of corrosion pits on the surface of the HA-coated materials could be related to the existence of some micropores in the coating layer that act as conducting paths between the corrosive medium and the metallic substrate.

These observations confirm the marked enhancement of the passive film and corrosion resistance after HA coating. According to the current results, the significant improvement of the corrosion resistance of the deformed 316Ti SS after HA coating together with the high mechanical properties offer promising advantages of the studied material for clinical applications.

4. Conclusions

The plastic deformation, through cold rolling, and HA coating were evaluated for their ability to improve the mechanical properties and corrosion resistance of 316Ti SS. The following conclusions can be drawn from this research.

- Compared to the non-deformed material, increasing the deformation degree led to a clear shift in the corrosion potential (E_{corr}) to the negative direction and an increase in the anodic current density (I_{corr}).
- Pit initiation frequency increased with the deformation degree.
- The formed HA coating was homogeneous and dense, and completely covered the underlying substrate material. The formed coating had an average Ca/P ratio of 1.63.
- The HA-coated surface revealed markedly higher roughness values compared to the grinded surface.
- HA coating resulted in a significant reduction of the corrosion current density. The corrosion current density (I_{corr}) and corrosion rate of the deformed material ($\varphi = 2.25$) dropped from 9980 $nA \cdot cm^{-2}$ and 3.09 mpy to 328 $nA \cdot cm^{-2}$ and 0.167 mpy, respectively.

Based on these conclusions; HA coating of the deformed 316Ti SS resulted in a combination of good mechanical properties and an excellent corrosion resistance, and hence acts as a promising implant material for biomedical applications.

References

[1] G. Manivasagam, D. Dhinasekaran, A. Rajamanickam, Biomedical implants: corrosion and its prevention — a review, Recent Pat. Corros. Sci. 2 (2010) 40–54.
[2] S. Kurtz, K. Ong, E. Lau, F. Mowat, M. Halpern, Projections of primary and revision hip and knee arthroplasty in the United States from 2005 to 2030, J. Bone Joint Surg. Am. 89 (2007) 780–785.
[3] A.J. Smith, P. Dieppe, K. Vernon, M. Porter, A.W. Blom, on behalf of the National Joint Registry of England and Wales, Lancet 379 (2012) 1199–1204.
[4] H.J. Rack, J.I. Qazi, Titanium alloys for biomedical applications, Mater. Sci. Eng. C 26 (2006) 1269–1277.
[5] M. Spector, Biomaterial failure, Orthop. Clin. N. Am. 23 (1992) 211–217.
[6] M. Navarro, A. Michiardi, O. Castaño, J.A. Panell, Review: biomaterials in orthopaedics, J. R. Soc. Interface 5 (2008) 1137–1158.
[7] J. Stráský, J. Havlíková, L. Bačáková, P. Harcuba, M. Mhaede, M. Janeček, Characterization of electric discharge machining, subsequent etching and shot-peening as a surface treatment for orthopaedic implants, Appl. Surf. Sci. 281 (2013) 73–78.
[8] S. Virtanen, I. Milošov, E. Gomez-barrenas, R. Trebše, J. Salo, Y.T. Konttinen, Special modes of corrosion under physiological and simulated physiological conditions, Acta Biomater. 4 (2008) 468–476.
[9] K. Meinert, C. Uerpmann, J. Matschullat, G.K. Wolf, Corrosion and leaching of silver doped ceramic IBAD coatings on SS 316L under simulated physiological conditions, Surf. Coat. Technol. 103–104 (1998) 58–65.
[10] C. Garcia, S. Cere, A. Duran, Bioactive coatings prepared by sol–gel on stainless steel 316 L, J. Non-Cryst. Solids 348 (2004) 218–224.
[11] S. Nagarajan, N. Rajendran, Surface characterisation and electrochemical behaviour of porous titanium dioxide coated 316L stainless steel for orthopaedic applications, Appl. Surf. Sci. 255 (2009) 3927–3932.
[12] G. Wang, H. Zreiqat, Functional coatings or films for hard-tissue applications, Materials 3 (2010) 3994–4050.
[13] B.R. Kumar, S. Sharma, B. Mahato, Formation of ultrafine grained microstructure in the austenitic stainless steel and its impact on tensile properties, Mater. Sci. Eng. A 528 (2011) 2209–2216.
[14] S. Rajasekhara, P.J. Ferreira, L.P. Karjalainen, A. Kyröläinen, Hall–Petch behavior in ultra-fine-grained AISI 301LN stainless steel, Metall. Mater. Trans. A 38 (2007) 1202–1210.
[15] Y. Ma, J.-E. Jin, Y.-K. Lee, A repetitive thermomechanical process to produce nanocrystalline in a metastable austenitic steel, Scr. Mater. 52 (2005) 1311–1315.
[16] A. Barbucci, M. Delucchi, M. Panizza, M. Sacco, G. Cerisola, Electrochemical and corrosion behaviour of cold rolled AISI 301 in 1 M H_2SO_4, J. Alloys Compd. 317–318 (2001) 607–611.

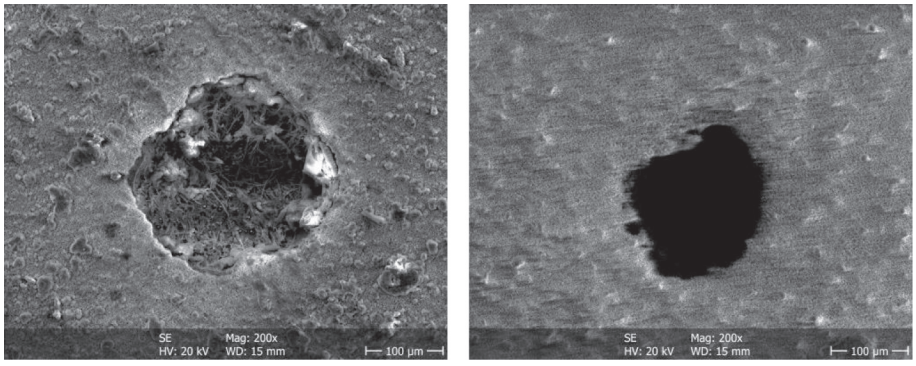

Fig. 10. SEM micrographs reveal the formation of corrosion pits on the HA-coated surfaces of SS 316Ti (a) non-deformed ($\varphi = 0$), and (b) deformed ($\varphi = 2.25$).

[17] R.D.K. Misra, B.R. Kumar, M. Somani, P. Karjalainen, Deformation processes during tensile straining of ultrafine/nanograined structures formed by reversion in metastable austenitic steels, Scr. Mater. 59 (2008) 79–88.
[18] A. Zeman, R. Novotny, O. Uca, V. Krsjak, J. Macak, L. Debarberis, Behavior of cold-worked AISI-304 steel in stress-corrosion cracking process: microstructural aspects, Appl. Surf. Sci. 255 (2008) 160–163.
[19] S.V. Phadnis, A.K. Satpati, K.P. Muthe, J.C. Vyas, R.I. Sudaresan, Comparison of rolled and heat treated SS304 in chloride solution using electrochemical and XPS techniques, Corros. Sci. 45 (2003) 2467–2483.
[20] M.K. Lei, X.M. Zhu, In vitro corrosion resistance of plasma source ion nitrided austenitic stainless steels, Biomaterials 22 (2001) 641–647.
[21] M. Sivakumar, S. Rajeswari, Investigation of failures in stainless steel orthopaedic implant devices: pit-induced stress corrosion cracking, J. Mater. Sci. Lett. 11 (1992) 1039–1042.
[22] S.P. Patterson, R.H. Daffner, R.A. Gallo, Electrochemical corrosion of metal implants, Am. J. Roentgenol. 184 (2005) 1219–1222.
[23] L. Sun, C.C. Berndt, K.A. Gross, A. Kucuk, Material fundamentals and clinical performance of plasma-sprayed hydroxyapatite coatings: a review, J. Biomed. Mater. Res. A 58 (2001) 570–592.
[24] B. Hadzima, M. Mhaede, F. Pastorek, Electrochemical characteristics of calcium-phosphatized AZ31 magnesium alloy in 0.9 % NaCl solution, J. Mater. Sci. Mater. Med. 25 (2014) 1227–1237.
[25] M. Mhaede, F. Pastorek, B. Hadzima, Influence of shot peening on corrosion properties of biocompatible magnesium alloy AZ31 coated by dicalcium phosphate dihydrate (DCPD), Mater. Sci. Eng. C 39 (2014) 330–335.
[26] J. Dumbleton, M.T. Manley, Hydroxyapatite-coated prostheses in total hip and knee arthroplasty, J. Bone Joint Surg. Am. 86 (2004) 2526–2540.
[27] R. Gadow, A. Killinger, N. Stiegler, Hydroxyapatite coatings for biomedical applications deposited by different thermal spray techniques, Surf. Coat. Technol. 205 (2010) 1157–1164.
[28] M. Schwind, J. Källqvist, J.-O. Nilsson, J. Ågren, H.-O. Andrèn, σ-Phase precipitation in stabilized austenitic stainless steels, Acta Mater. 48 (2000) 2473–2481.
[29] M. Najdoski, P. Majhi, I.S. Grozdanov, A simple chemical method for preparation of hydroxyapatite coatings on Ti6Al4V, J. Mater. Sci. Mater. Med. 12 (2001) 479–483.
[30] ASTM G5-94, Standard Reference Test Method for Making Potentiostatic and Potentiodynamic Anodic Polarization Measurements, ASTM, Philadelphia, 2004.
[31] A. Carreon-Alvarez, R. Castañeda-Valderrama, J. Avalos Martínez, A. Estrada-Vargas, S. Gómez-Salazar, M. Barcena-Soto, N. Casillas, Corrosion of aluminum, copper, brass and stainless steel 304 in tequila, Int. J. Electrochem. Sci. 7 (2012) 7877–7887.
[32] T.-H. Lee, E. Shin, C.-S. Oh, H.-Y. Ha, S.-J. Kim, Correlation between stacking fault energy and deformation microstructure in high-interstitial-alloyed austenitic steels, Acta Mater. 58 (2010) 3173–3186.
[33] J. Talonen, H. Hänninen, Formation of shear bands and strain-induced martensite during plastic deformation of metastable austenitic stainless steels, Acta Mater. 55 (2007) 6108–6118.
[34] T. Angel, Formation of martensite in austenitic stainless steel, J. Iron Steel Inst. 177 (1954) 165–174.
[35] L.-H. Lee, J.-S. Ha, Deposition behavior and characteristics of hydroxyapatite coatings on Al_2O_3, Ti, and Ti6Al4V formed by a chemical bath method, Ceram. Int. 40 (2014) 5321–5326.
[36] M.J. Filiaggi, R.M. Pilliar, N.A. Coombs, Post-plasma-spraying heat treatment of the HA coating/Ti-6A1-4V implant system, J. Biomed. Mater. Res. A 27 (1993) 191–198.
[37] H. Ji, P.M. Marquis, Effect of heat treatment on the microstructure of plasma-sprayed hydroxyapatite coating, Biomaterials 14 (1993) 64–68.
[38] D.D. Deligianni, N. Katsala, S. Ladas, D. Sotiropoulou, J. Amedee, Y.F. Missirlis, Effect of surface roughness of the titanium alloy Ti-6Al-4V on human bone marrow cell response and on protein adsorption, Biomaterials 22 (2001) 1241–1251.
[39] D.O. Costa, P.D.H. Prowse, T. Chrones, S.M. Sims, D.W. Hamilton, A.S. Rizkalla, S.J. Dixon, The differential regulation of osteoblast and osteoclast activity by surface topography of hydroxyapatite coatings, Biomaterials 34 (2013) 7215–7226.
[40] S.V. Dorozhkin, Calcium orthophosphates: occurrence, properties, biomineralization, pathological calcification and biomimetic applications, Biomaterials 1 (2011) 121–164.
[41] L. Peguet, B. Malki, B. Baroux, Influence of cold working on the pitting corrosion resistance of stainless steels, Corros. Sci. 49 (2007) 1933–1948.
[42] U.K. Mudali, P. Shankar, S. Ningshen, R.K. Dayal, H.S. Khatak, B. Raj, On the pitting corrosion resistance of nitrogen alloyed cold worked austenitic stainless steels, Corros. Sci. 44 (2002) 2183–2198.
[43] A. Barbucci, G. Cerisola, P.L. Cabotb, Effect of cold-working in the passive behavior of 304 stainless steel in sulfate media, J. Electrochem. Soc. 149 (2002) B534–B542.
[44] E. Symniotis, Galvanic effects on the active dissolution of duplex stainless steels, Corrosion 46 (1990) 2–11.
[45] Y.-H. Yau, M.A. Streicher, Galvanic corrosion of duplex FeCr-10% Ni alloys in reducing acids, Corrosion 43 (1987) 366–373.
[46] R. Ke, R. Alkire, Initiation of corrosion pits at inclusions on 304 stainless steel, J. Electrochem. Soc. 142 (1995) 4056–4062.
[47] B. Aksakal, M. Gavgali, B. Dikici, The effect of coating thickness on corrosion resistance of hydroxyapatite coated Ti6Al4V and 316L SS implants, J. Mater. Eng. Perform. 19 (2010) 894–899.
[48] S. Sonmez, B. Aksakal, B. Dikici, Influence of hydroxyapatite coating thickness and powder particle size on corrosion performance of MA8M magnesium alloy, J. Alloys Compd. 596 (2014) 125–131.
[49] C.P.A.T. Klein, J.G.C. Wolke, J.M.A. de Blieck-Hogervorst, K. de Groot, Features of calcium phosphate plasma-sprayed coatings: an *in vitro* study, J. Biomed. Mater. Res. A 28 (1994) 961–967.
[50] L. Chou, B. Marek, W.R. Wagner, Effects of hydroxylapatite coating crystallinity on biosolubility, cell attachment efficiency and proliferation *in vitro*, Biomaterials 20 (1999) 977–985.
[51] G.L. Darimont, R. Cloots, E. Heinen, L. Seidel, R. Legrand, *In vivo* behavior of hydroxyapatite coatings on tiyanium implants: a quantitative study in the rabbit, Biomaterials 23 (2002) 2569–2575.
[52] W. Xue, S. Tao, X. Liu, X. Zheng, C. Ding, *In vivo* evaluation of plasma sprayed hydroxyapatite coatings having different crystallinity, Biomaterials 25 (2004) 415–421.
[53] W. Xue, X. Liu, X. Zheng, C. Ding, Effect of hydroxyapatite coating crystallinity on dissolution and osseointegration in vivo, J. Biomed. Mater. Res. A 74 (2005) 553–561.
[54] D. Gopi, J. Indira, L. Kavitha, J.M.F. Ferreira, Hydroxyapatite coating on selectively passivated and sensitively polymer-protected surgical grade stainless steel, J. Appl. Electrochem. 43 (2013) 331–345.